JOURNAL OF THEORETICAL
AND APPLIED MECHANICS
https://doi.org/10.15632/jtam-pl/239002
ONLINE FIRST

AN IMPROVED ALTERNATING DIRECTION IMPLICIT DIFFERENCE SOLUTION FOR 2D PLANE STRAIN MULTIPHASE COUPLED STEADY-STATE DIFFUSION EQUATIONS

Qian HE[1,2], Longqi LI[1,2*], Yaping YANG[1], Quan YUAN[3], Canghao DONG[1]

[1] *College of Environmental and Civil Engineering, Chengdu University of Technology, Chengdu, China*
[2] *State Key Laboratory of Geohazard Prevention and Geoenvironment Protection, Chengdu University of Technology, Chengdu, China*
[3] *School of Architecture and Civil Engineering, Xihua University, Chengdu, China*
[*]corresponding author, *lilongqi2014@cdut.edu.cn*

Two-dimensional multiphase coupling problems are ubiquitous in diverse research domains. However, when it comes to problems involving higher dimensions and multi-physics coupling, existing solutions struggle to provide even a preliminary prediction. This study proposes an improved alternating direction implicit (IADI) difference algorithm to solve these problems. A conventional difference mesh is first split and then reassembled into a new mesh that couples the individual phases. A virtual mesh is constructed on adjacent time layers, with the iteration between the virtual and real meshes carried out via matrix operations. The IADI solution has high computational efficiency and accuracy in a series of examples.

Keywords: two-dimensional plane strain; virtual grid method; IADI solution; stability; multiphase coupling.



Articles in JTAM are published under Creative Commons Attribution 4.0 International.
Unported License https://creativecommons.org/licenses/by/4.0/deed.en.
By submitting an article for publication, the authors consent to the grant of the said license.

1. Introduction

Parabolic partial differential equations (PDEs) are frequently encountered in the study of heat conduction processes, gas diffusion phenomena, soil consolidation, and electromagnetic field propagation (Thomas, 1999). Parabolic equations also constitute one of the most important and widely applied branches of the theory of PDEs. The application of parabolic PDEs permeates nearly every corner of modern science. In physics and engineering, they describe heat conduction, mass diffusion, viscous fluid flow, and the diffusion of electromagnetic fields in conducting media (Sharifi & Rashidinia, 2016). In materials science, the governing equations for phase-change problems, such as the Stefan problem, also fall into the parabolic category (Myers *et al.*, 2020). In biology, the spatial spread of populations, tumor growth, and the transmission of neural signals can be modeled using systems of reaction-diffusion equations (Perthame, 2015). In geotechnical engineering, these equations governing the air and water phases are employed to describe the transient flow of the water phase in saturated soils and of both phases in unsaturated soils (Dakshanamurthy & Fredlund, 1980; Yuan *et al.*, 2023).

Parabolic PDEs involve first-order temporal derivatives and second-order spatial derivatives. Solving such equations generally requires initial conditions (specifying the distribution at the initial instant) and boundary conditions (describing the interaction between the system and its surroundings). For a one-dimensional parabolic partial differential equation, the separation of variables (Shan *et al.*, 2012), eigenfunction (Yuan *et al.*, 2023), Laplace transform and inverse Laplace transform (Wang *et al.*, 2019), explicit difference (Fredlund & Hasan, 1979), differential quadrature (Zhou & Zhao, 2014), implicit difference (Singh & Chakraborty, 2024; He *et al.*, 2025a), and transformed differential quadrature methods (Kou *et al.*, 2026) can readily obtain

the solution of PDEs. Most practical problems involve higher dimensions (i.e., two- and three-dimensional) and a larger number of coupled phases, which inevitably results in greater computational difficulty and increased computational expense. Although the explicit difference and transformed differential quadrature methods are available in some published works for solving two-phase coupling problems in two-dimensional unsaturated soils, their procedural complexity and low computational efficiency inevitably result in higher computational costs. Therefore, it is very necessary to develop an algorithm with high computational efficiency and reliability to solve the multiphysics coupling problem.

Based on the heat conduction equation, the consolidation equation for unsaturated soils, and the solute migration equation, this paper proposes a system of multiphase-coupled parabolic PDEs. An improved alternating direction implicit (IADI) scheme is developed for the two-dimensional problems with multiple physical quantities. A new mesh is formed by combining the explicit difference meshes of the different physical quantities, and the matrix iteration is performed between the virtual mesh and the real mesh to obtain numerical solutions. Two examples containing both analytical and numerical solutions are proposed to demonstrate the effectiveness and accuracy of the IADI solution. Based on the verified numerical solution, a series of examples was carried out to illustrate the influence of the boundary condition and x/z direction permeability ratio on the behavior of the model.

2. Mathematical model

2.1. Governing equations

The model that can describe the two-dimensional multiphase coupling problem is shown in Fig. 1. The model with the length L and thickness H is subjected to external loading, wherein $b_{11}, b_{22}, ..., b_{ii}$, $c_{11}, c_{22}, ..., c_{ii}$ are parameters along the x- and z-directions. It should be noted that, in different fields, certain assumptions are required for the formulation of the corresponding system of PDEs (Terzaghi, 1943; Fredlund & Hasan, 1979).

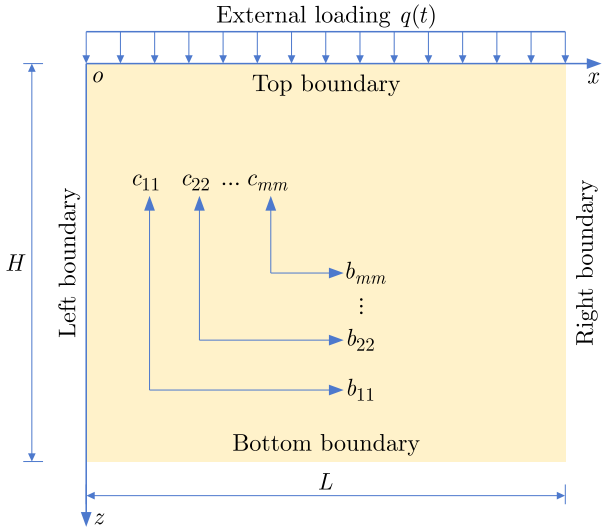


Fig. 1. Simple schematic diagram of a two-dimensional model.

Seepage, diffusion, heat conduction, soil consolidation, and other engineering physics problems frequently involve solving initial-boundary value problems of parabolic PDEs. The two-dimensional model of such problems is as follows:

$$\mathbf{E}\frac{\partial \mathbf{u}}{\partial t} + \mathbf{X}\frac{\partial^2 \mathbf{u}}{\partial x^2} + \mathbf{Z}\frac{\partial^2 \mathbf{u}}{\partial z^2} = \frac{\partial \mathbf{f}}{\partial t}, \tag{2.1}$$

where

$$\mathbf{u}=\begin{bmatrix} u_1(x,z,t) \\ u_2(x,z,t) \\ \vdots \\ u_m(x,z,t) \end{bmatrix}, \quad \mathbf{E}=\begin{pmatrix} 1 & a_{12} & \cdots & a_{1m} \\ a_{21} & 1 & \cdots & a_{2m} \\ \vdots & \vdots & \ddots & \vdots \\ a_{m1} & a_{m2} & \cdots & 1 \end{pmatrix}, \quad \mathbf{X}=\begin{pmatrix} b_{11} & 0 & \cdots & 0 \\ 0 & b_{22} & \cdots & 0 \\ \vdots & \vdots & \ddots & \vdots \\ 0 & 0 & \cdots & b_{mm} \end{pmatrix},$$

$$\mathbf{Z}=\begin{pmatrix} c_{11} & 0 & \cdots & 0 \\ 0 & c_{22} & \cdots & 0 \\ \vdots & \vdots & \ddots & \vdots \\ 0 & 0 & \cdots & c_{mm} \end{pmatrix}, \quad \mathbf{f}=\begin{bmatrix} f_1 \\ f_2 \\ \vdots \\ f_m \end{bmatrix} f(x,z,t).$$

In Eq. (2.1), $a_{12}, a_{13}, \cdots$ are coupling coefficients, which may be either constants or functions of time, t; $b_{11}, b_{22}, ..., b_{mm}$, $c_{11}, c_{22}, ..., c_{mm}$ can be either constants or functions of the x- and z-coordinates; $f_1, f_2, ..., f_m$ are constants; $f(x,z,t)$ is a function of the x-coordinate, z-coordinate, and time, t.

2.2. Boundary and initial conditions

To obtain a closed-form solution of the two-dimensional governing equations, boundary and initial conditions must be prescribed. A two-dimensional model contains the edge and point boundary conditions. There are three main types of boundary conditions, i.e., the Dirichlet boundary (DB) condition, the Neumann boundary (NB) condition, and the Robin boundary (RB) condition (Thomas, 1999).

2.2.1. Edge boundary condition

The boundary conditions for four edges are

$$\text{DB}: \mathbf{u}|_{\text{edge}} = \mathbf{0}, \tag{2.2}$$

$$\text{NB}: \left.\frac{\partial \mathbf{u}}{\partial x}\right|_{\text{edge}} = \mathbf{0}, \qquad \left.\frac{\partial \mathbf{u}}{\partial z}\right|_{\text{edge}} = \mathbf{0}, \tag{2.3}$$

$$\text{RB}: \left.\frac{\partial \mathbf{u}}{\partial x}\right|_{\text{edge}} = \pm\mathbf{R}\mathbf{u}|_{\text{edge}}, \qquad \left.\frac{\partial \mathbf{u}}{\partial z}\right|_{\text{edge}} = \pm\mathbf{R}\mathbf{u}|_{\text{edge}}, \tag{2.4}$$

where edge denotes the edge corresponding to the model;

$$\mathbf{R}=\begin{pmatrix} r_{11} & 0 & \cdots & 0 \\ 0 & r_{22} & \cdots & 0 \\ \vdots & \vdots & \ddots & \vdots \\ 0 & 0 & \cdots & r_{mm} \end{pmatrix}; \qquad r_{11}, r_{22}, ..., r_{mm} \quad \text{are the constants.}$$

It is noteworthy that when r_{mm} =0, the RB condition can degenerate into the NB condition; conversely, when r_{mm} tends to infinity, the RB condition can approximate the DB condition (Singh & Chakraborty, 2024). However, some numerical examples indicate that when the values of $r_{11}, r_{22}, ..., r_{mm}$ are set to 100, the computational results under the RB condition agree with those under the DB condition (He et al., 2025b). Therefore, when r_{mm} is greater than 100, the following equation can be obtained:

$$\left.\frac{\partial \mathbf{u}}{\partial x}\right|_{\text{edge}} = \pm\mathbf{R}\mathbf{u}|_{\text{edge}} \rightarrow \mathbf{u}|_{\text{edge}} = 0 \quad (r_{11}, r_{22}, ..., r_{nn} > 100), \tag{2.5}$$

$$\left.\frac{\partial \mathbf{u}}{\partial z}\right|_{\text{edge}} = \pm\mathbf{R}\mathbf{u}|_{\text{edge}} \rightarrow \mathbf{u}|_{\text{edge}} = 0 \quad (r_{11}, r_{22}, ..., r_{nn} > 100). \tag{2.6}$$

2.2.2. Point boundary condition

Two intersecting edges will create a new point; the point boundary must meet the drainage conditions of two adjacent edges. The boundary conditions at the four points in the two-dimensional model are

$$\mathbf{u}|_{\text{point}} = 0, \tag{2.7}$$

$$\begin{cases} \left.\dfrac{\partial \mathbf{u}}{\partial x}\right|_{\text{point}} = \mathbf{0}, \\ \left.\dfrac{\partial \mathbf{u}}{\partial z}\right|_{\text{point}} = \mathbf{0}, \end{cases} \quad \begin{cases} \left.\dfrac{\partial \mathbf{u}}{\partial x}\right|_{\text{point}} = \mathbf{0}, \\ \left.\dfrac{\partial \mathbf{u}}{\partial z}\right|_{\text{point}} = \pm \mathbf{R}\mathbf{u}|_{\text{point}}, \end{cases}$$

$$\begin{cases} \left.\dfrac{\partial \mathbf{u}}{\partial x}\right|_{\text{point}} = \pm \mathbf{R}\mathbf{u}|_{\text{point}}, \\ \left.\dfrac{\partial \mathbf{u}}{\partial z}\right|_{\text{point}} = \mathbf{0}, \end{cases} \quad \begin{cases} \left.\dfrac{\partial \mathbf{u}}{\partial x}\right|_{\text{point}} = \pm \mathbf{R}\mathbf{u}|_{\text{point}}, \\ \left.\dfrac{\partial \mathbf{u}}{\partial z}\right|_{\text{point}} = \pm \mathbf{R}\mathbf{u}|_{\text{point}}, \end{cases} \tag{2.8}$$

where point denotes the point corresponding to the model.

The initial conditions are expressed as

$$\mathbf{u}(x, z, 0) = g(x, z) \begin{bmatrix} u_1^0 \\ u_2^0 \\ \vdots \\ u_m^0 \end{bmatrix}, \tag{2.9}$$

where $u_1^0, u_2^0, ..., u_m^0$ are the initial values at $t = 0$; $g(x, z)$ is a function of x and z.

3. IADI difference solution

According to the previous literature, the finite difference method was widely utilized to solve PDEs. Fredlund & Hasan (1979) first applied the explicit difference program to solve the consolidation equations of unsaturated soil. Feng *et al.* (2019) applied the implicit difference method to verify the correctness of the developed solution; He *et al.* (2025b) employed it in the optimization of sand cushion layers. These applications demonstrate that the finite difference method is applicable to solving various types of PDEs. Although analytical solutions exist for some PDEs, they are generally difficult to obtain for multiphase coupling problems (Shan *et al.*, 2012; Yuan *et al.*, 2023). Therefore, it is necessary to develop a finite difference method specifically tailored to multiphase coupling problems.

3.1. Discretization of governing equations

The implicit difference solution for the one-dimensional consolidation equations involves two-dimensional matrix iteration (He *et al.*, 2026a). Similarly, the transformation of a three-dimensional matrix occurs in the implicit difference solution of two-dimensional consolidation equations. The increase in computational dimensions will lead to a more tedious iterative process. To improve the calculation accuracy of the algorithm, an alternating direction implicit (ADI) solution is introduced to discretize Eq. (2.1). The ADI method, established by Peaceman and Rachford (Thomas, 1995), has been widely applied to solve two-dimensional PDEs. It should be noted, however, that Eq. (2.1) is a system of PDEs, and the ADI method cannot be used directly. This is because the iterative matrix for a system of PDEs is more complex and variable

than that for a single PDE. Moreover, the matrix formed by the unknown vectors is not square. Therefore, we have conducted a secondary development of the ADI algorithm, enabling it to solve systems of PDEs involving two or more physical quantities.

As shown in Fig. 2, the key idea of the IADI scheme is to construct a virtual time layer, $t_{n+1/2}$, between layers t_n and t_{n+1}. The IADI algorithm requires two iterations in one time step; it is also known as the two-step method. In Fig. 2, the time and spatial domains are respectively divided into N, J, and K equidistant nodes; the time and space steps are τ, h_x, and h_z; the node coordinates are (x_j, z_k, t_n), and $t_n = n\tau$, $n = 0, 1, 2, ..., N$, $x_j = jh_x$, $j = 0, 1, 2, ..., J$, $z_k = kh_z$, $k = 0, 1, 2, ..., K$.

Step 1, at time step $t_n \sim t_{n+1/2}$, Eq. (2.1) is implicitly discretized in the x-direction, yielding

$$\mathbf{E}\frac{\mathbf{u}_{jk}^{n+\frac{1}{2}} - \mathbf{u}_{jk}^{n}}{\tau/2} + \mathbf{X}\frac{\delta_x^2 \mathbf{u}_{jk}^{n+\frac{1}{2}}}{h_x^2} + \mathbf{Z}\frac{\delta_z^2 \mathbf{u}_{jk}^{n}}{h_z^2} = \frac{\mathbf{f}^{n+\frac{1}{2}} - \mathbf{f}^{n}}{\tau/2}, \tag{3.1}$$

where

$$\delta_x^2 \mathbf{u}_{jk}^{n+\frac{1}{2}} = \mathbf{u}_{(j-1)k}^{n+\frac{1}{2}} - 2\mathbf{u}_{jk}^{n+\frac{1}{2}} + \mathbf{u}_{(j+1)k}^{n+\frac{1}{2}}, \qquad \delta_z^2 \mathbf{u}_{jk}^{n} = \mathbf{u}_{j(k-1)}^{n} - 2\mathbf{u}_{jk}^{n} + \mathbf{u}_{j(k+1)}^{n}.$$

Equation (3.1) can be rewritten as

$$\begin{aligned} &2\lambda_x \mathbf{X}\mathbf{u}_{(j-1)k}^{n+\frac{1}{2}} + (\mathbf{E} - 4\lambda_x \mathbf{X})\mathbf{u}_{jk}^{n+\frac{1}{2}} + 2\lambda_x \mathbf{X}\mathbf{u}_{(j+1)k}^{n+\frac{1}{2}} \\ &\qquad = -2\lambda_z \mathbf{Z}u_{j(k-1)}^{n} + (\mathbf{E} + 4\lambda_z \mathbf{Z})u_{jk}^{n} - 2\lambda_z \mathbf{Z}u_{j(k+1)}^{n} + \mathbf{f}^{n+\frac{1}{2}} - \mathbf{f}^{n}, \end{aligned} \tag{3.2}$$

where $\lambda_x = \tau/h_x^2$, $\lambda_z = \tau/h_z^2$; λ_x and λ_z are the mesh ratios; $\lambda_x = H^2\lambda_z/L^2$, and $J = K = C$ (C is a natural number).

In this study, we define two matrices, $\mathbf{U}$ and $\mathbf{V}$, at time layers $t_{n+1/2}$ and t_n, where $\mathbf{U}$ and $\mathbf{V}$ are $mC \times C$ matrices. Then, Eq. (3.2) can be written as

$$\mathbf{AU} = \mathbf{BV}, \tag{3.3}$$

where

$$\mathbf{A} = \begin{pmatrix} 1-4\lambda_x b_{11} & a_{12} & 2\lambda_x b_{11} & a_{13} & \cdots & 0 & 0 \\ a_{21} & 1-4\lambda_x b_{22} & a_{23} & 2\lambda_x b_{22} & \cdots & 0 & 0 \\ 2\lambda_x b_{33} & a_{32} & 1-4\lambda_x b_{33} & a_{34} & \cdots & 0 & 0 \\ \vdots & \vdots & \vdots & \ddots & \vdots & \vdots & \vdots \\ 0 & 0 & 0 & \cdots & 1-4\lambda_x b_{(m-2)(m-2)} & a_{(m-2)(m-1)} & 2\lambda_x b_{(m-2)(m-2)} \\ 0 & 0 & 0 & \cdots & a_{(m-1)(m-2)} & 1-4\lambda_x b_{(m-1)(m-1)} & a_{(m-1)m} \\ 0 & 0 & 0 & \cdots & 2\lambda_x b_{mm} & a_{m(m-1)} & 1-4\lambda_x b_{mm} \end{pmatrix},$$

$$\mathbf{B} = \begin{pmatrix} 1+4\lambda_z c_{11} & a_{12} & -2\lambda_z c_{11} & a_{13} & \cdots & 0 & 0 \\ a_{21} & 1+4\lambda_z c_{22} & a_{23} & -2\lambda_z c_{22} & \cdots & 0 & 0 \\ -2\lambda_z c_{33} & a_{32} & 1+4\lambda_z c_{33} & a_{34} & \cdots & 0 & 0 \\ \vdots & \vdots & \vdots & \ddots & \vdots & \vdots & \vdots \\ 0 & 0 & 0 & \cdots & 1+4\lambda_z c_{(m-2)(m-2)} & a_{(m-2)(m-1)} & -2\lambda_z c_{(m-2)(m-2)} \\ 0 & 0 & 0 & \cdots & a_{(m-1)(m-2)} & 1+4\lambda_z c_{(m-1)(m-1)} & a_{(m-1)m} \\ 0 & 0 & 0 & \cdots & -2\lambda_z c_{mm} & a_{m(m-1)} & 1+4\lambda_z c_{mm} \end{pmatrix},$$

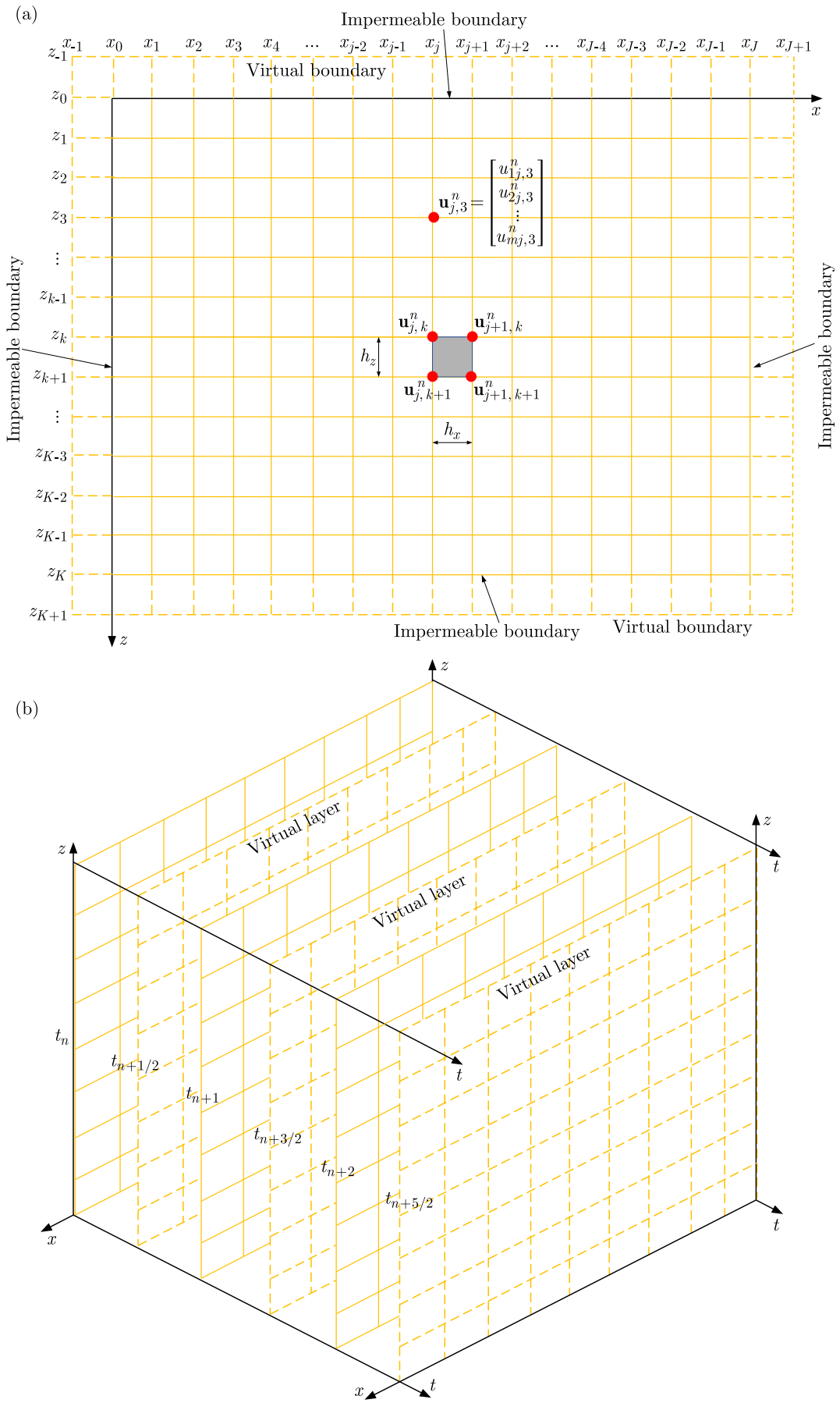


Fig. 2. Difference mesh of IADI scheme: (a) construction of mesh; (b) iterative process.

$$\mathbf{U}=\begin{pmatrix} (u_1)_{11}^{n+1/2} & (u_1)_{12}^{n+1/2} & \cdots & (u_1)_{1K-1}^{n+1/2} & (u_1)_{1K}^{n+1/2} \\ (u_2)_{11}^{n+1/2} & (u_2)_{11}^{n+1/2} & \cdots & (u_2)_{1K-1}^{n+1/2} & (u_2)_{1K}^{n+1/2} \\ \vdots & \vdots & \cdots & \vdots & \vdots \\ (u_1)_{21}^{n+1/2} & (u_1)_{22}^{n+1/2} & \cdots & (u_2)_{2K-1}^{n+1/2} & (u_2)_{2K}^{n+1/2} \\ \vdots & \vdots & \cdots & \vdots & \vdots \\ (u_m)_{J1}^{n+1/2} & (u_m)_{J2}^{n+1/2} & \cdots & (u_m)_{JK-1}^{n+1/2} & (u_m)_{JK}^{n+1/2} \end{pmatrix},$$

$$\mathbf{V}=\begin{pmatrix} (u_1)_{11}^{n} & (u_1)_{12}^{n} & \cdots & (u_1)_{1K-1}^{n} & (u_1)_{1K}^{n} \\ (u_2)_{11}^{n} & (u_2)_{11}^{n} & \cdots & (u_2)_{1K-1}^{n} & (u_2)_{1K}^{n} \\ \vdots & \vdots & \cdots & \vdots & \vdots \\ (u_1)_{21}^{n} & (u_1)_{22}^{n} & \cdots & (u_2)_{2K-1}^{n} & (u_2)_{2K}^{n} \\ \vdots & \vdots & \cdots & \vdots & \vdots \\ (u_m)_{J1}^{n} & (u_m)_{J2}^{n} & \cdots & (u_m)_{JK-1}^{n} & (u_m)_{JK}^{n} \end{pmatrix},$$

$\mathbf{A}$ and $\mathbf{B}$ are $(2m+1)$-diagonal sparse matrices.

Step 2, at time step $t_{n+\frac{1}{2}} \sim t_{n+1}$, Eq. (2.1) is implicitly discretized in the z-direction; we obtain:

$$\mathbf{E}\frac{\mathbf{u}_{jk}^{n+1}-\mathbf{u}_{jk}^{n+\frac{1}{2}}}{\tau/2}+\mathbf{X}\frac{\delta_x^2\mathbf{u}_{jk}^{n+\frac{1}{2}}}{h_x^2}+\mathbf{Z}\frac{\delta_z^2\mathbf{u}_{jk}^{n+1}}{h_z^2}=\frac{\mathbf{f}^{n+1}-\mathbf{f}^{n+\frac{1}{2}}}{\tau/2}. \tag{3.4}$$

Similarly, Eq. (3.4) can be rewritten as

$$\begin{aligned} &2\lambda_z\mathbf{Z}\mathbf{u}_{j(k-1)}^{n+1}+(\mathbf{E}-4\lambda_z\mathbf{Z})\mathbf{u}_{jk}^{n+1}+2\lambda_z\mathbf{Z}\mathbf{u}_{j(k+1)}^{n+1} \\ &\qquad=-2\lambda_x\mathbf{X}\mathbf{u}_{(j-1)k}^{n+\frac{1}{2}}+(\mathbf{E}+4\lambda_x\mathbf{X})\mathbf{u}_{jk}^{n+\frac{1}{2}}-2\lambda_x\mathbf{X}\mathbf{u}_{(j+1)k}^{n+\frac{1}{2}}+\mathbf{f}^{n+1}-\mathbf{f}^{n+\frac{1}{2}}. \end{aligned} \tag{3.5}$$

In the first iteration, only numerical iterations in the x-direction are involved. For a single equation, $\mathbf{U}$ is a $C\times C$ matrix, and it can be used as the initial value for the second iteration in the z-direction by the matrix transposition. However, $\mathbf{U}$ is an $mC\times C$ matrix in Eq. (3.3) and cannot be used directly in the second iteration algorithm. Only after the matrix $\mathbf{U}$ is reconstructed can it be used as the initial value of the second iteration. Then, Eq. (3.5) is written as

$$\mathbf{CV}=\mathbf{DU}, \tag{3.6}$$

where

$$\mathbf{C}=\begin{pmatrix} 1-4\lambda_z c_{11} & a_{12} & 2\lambda_z c_{11} & a_{13} & \cdots & 0 & 0 \\ a_{21} & 1-4\lambda_z c_{22} & a_{23} & 2\lambda_z c_{22} & \cdots & 0 & 0 \\ 2\lambda_z c_{33} & a_{32} & 1-4\lambda_z c_{33} & a_{34} & \cdots & 0 & 0 \\ \vdots & \vdots & \vdots & \ddots & \vdots & \vdots & \vdots \\ 0 & 0 & 0 & \cdots & 1-4\lambda_z c_{(m-2)(m-2)} & a_{(n-2)(n-1)} & 2\lambda_z c_{(m-2)(m-2)} \\ 0 & 0 & 0 & \cdots & a_{(m-1)(m-2)} & 1-4\lambda_z c_{(m-1)(m-1)} & a_{(m-1)m} \\ 0 & 0 & 0 & \cdots & 2\lambda_z c_{mm} & a_{m(m-1)} & 1-4\lambda_z c_{mm} \end{pmatrix},$$

$$\mathbf{D}=\begin{pmatrix} 1+4\lambda_x b_{11} & a_{12} & -4\lambda_x b_{11} & a_{13} & \cdots & 0 & 0 \\ a_{21} & 1+4\lambda_x b_{22} & a_{23} & -4\lambda_x b_{22} & \cdots & 0 & 0 \\ -4\lambda_x b_{33} & a_{32} & 1+4\lambda_x b_{33} & a_{34} & \cdots & 0 & 0 \\ \vdots & \vdots & \vdots & \ddots & \vdots & \vdots & \vdots \\ 0 & 0 & 0 & \cdots & 1+4\lambda_x b_{(m-2)(m-2)} & a_{(n-2)(n-1)} & -4\lambda_x b_{(m-2)(m-2)} \\ 0 & 0 & 0 & \cdots & a_{(m-1)(m-2)} & 1+4\lambda_x b_{(m-1)(m-1)} & a_{(m-1)m} \\ 0 & 0 & 0 & \cdots & -4\lambda_x b_{mm} & a_{m(m-1)} & 1+4\lambda_x b_{mm} \end{pmatrix},$$

$$\mathbf{V}=\begin{pmatrix} (u_1)_{11}^{n+1} & (u_1)_{21}^{n+1} & \cdots & (u_1)_{(J-1)1}^{n+1} & (u_1)_{J1}^{n+1} \\ (u_2)_{11}^{n+1} & (u_2)_{21}^{n+1} & \cdots & (u_2)_{(J-1)1}^{n+1} & (u_2)_{J1}^{n+1} \\ \vdots & \vdots & \cdots & \vdots & \vdots \\ (u_1)_{12}^{n+1} & (u_1)_{22}^{n+1} & \cdots & (u_1)_{(J-1)2}^{n+1} & (u_1)_{J2}^{n+1} \\ \vdots & \vdots & \cdots & \vdots & \vdots \\ (u_m)_{1K}^{n+1} & (u_m)_{2K}^{n+1} & \cdots & (u_m)_{(J-1)K}^{n+1} & (u_m)_{JK}^{n+1} \end{pmatrix},$$

$$\mathbf{U}=\begin{pmatrix} (u_1)_{11}^{n+1/2} & (u_1)_{21}^{n+1/2} & \cdots & (u_1)_{(J-1)1}^{n+1/2} & (u_1)_{J1}^{n+1/2} \\ (u_2)_{11}^{n+1/2} & (u_2)_{21}^{n+1/2} & \cdots & (u_2)_{(J-1)1}^{n+1/2} & (u_2)_{J1}^{n+1/2} \\ \vdots & \vdots & \cdots & \vdots & \vdots \\ (u_1)_{12}^{n+1/2} & (u_1)_{22}^{n+1/2} & \cdots & (u_2)_{(J-1)2}^{n+1/2} & (u_2)_{J2}^{n+1/2} \\ \vdots & \vdots & \cdots & \vdots & \vdots \\ (u_m)_{1K}^{n+1/2} & (u_m)_{2K}^{n+1/2} & \cdots & (u_m)_{(J-1)K}^{n+1/2} & (u_m)_{JK}^{n+1/2} \end{pmatrix},$$

C and **D** are $(2m+1)$-diagonal sparse matrices.

In Eq. (3.6), **U** is a reconstructed matrix. After the second iteration, it is necessary to reconstruct the **V** matrix again. By repeating this iterative program, the distribution of $u_1, u_2, ..., u_m$ at an arbitrary time layer can be obtained. It is worth noting that the steps of discretizing along the x-direction and along the z-direction can be interchanged without any influence on the final numerical results.

3.2. Discretization of boundary and initial conditions

As shown in Fig. 3a, when the edge boundary and point boundary satisfy the DB condition, i.e., Eq. (2.2), Eq. (2.5), Eq. (2.6), and Eq. (2.7), the boundary values can be directly substituted into Eq. (3.2) and Eq. (3.4). On the other hand, when the edge boundary and point boundary are designated as the NB and RB conditions, such as Eq. (2.3) and Eq. (2.4), the virtual mesh method (Morton & Mayers, 2005) is utilized to obtain the discrete scheme at the boundary.

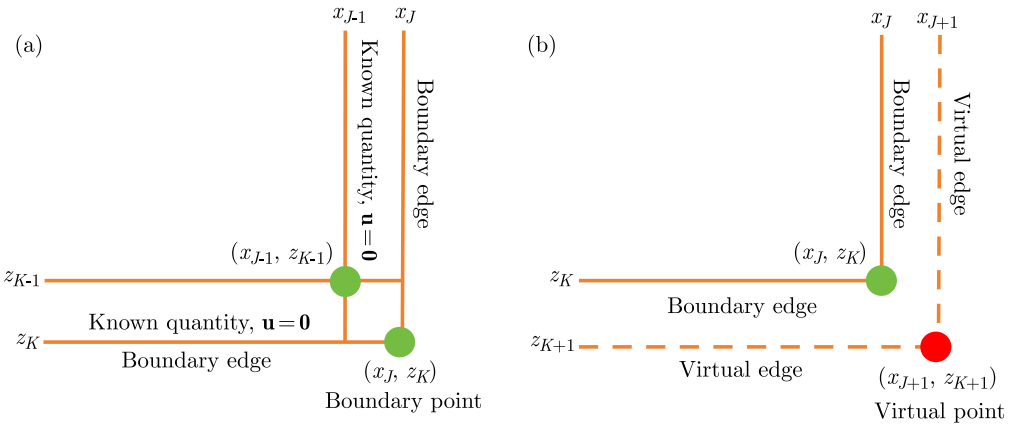


Fig. 3. Difference mesh at boundary: (a) permeable boundary, (b) impermeable boundary.

As shown in Fig. 3b, two virtual edges are constructed outside the boundary. These two virtual edges create a virtual point (red point). Based on these virtual edges and points, Eq. (2.3) and Eq. (2.4) are discretized as

$$\frac{\mathbf{u}_{j(K+1)}^n-\mathbf{u}_{j(K-1)}^n}{2h_z}=\mathbf{0}, \qquad \frac{\mathbf{u}_{(J+1)k}^n-\mathbf{u}_{(J-1)k}^n}{2h_x}=\mathbf{0}, \tag{3.7}$$

$$\frac{\mathbf{u}_{j(K+1)}^n-\mathbf{u}_{j(K-1)}^n}{2h_z}=\pm\mathbf{R}\mathbf{u}_{jK}^n, \qquad \frac{\mathbf{u}_{(J+1)k}^n-\mathbf{u}_{(J-1)k}^n}{2h_x}=\pm\mathbf{R}\mathbf{u}_{Jk}^n. \tag{3.8}$$

The discrete form of points and the discrete form of boundaries are consistent. The IADI solution at the boundary is obtained by substituting Eq. (3.7) and Eq. (3.8) into Eq. (3.2) and Eq. (3.5) to eliminate the virtual edges and points.

After obtaining the discrete scheme of the boundary conditions and consolidation equations, the final IADI solution can be represented as

$$\mathbf{\Phi}_1\mathbf{U} = \mathbf{\Phi}_2\mathbf{V}, \tag{3.9}$$

$$\mathbf{\Phi}_3\mathbf{V} = \mathbf{\Phi}_4\mathbf{U}, \tag{3.10}$$

where $\mathbf{\Phi}_1$, $\mathbf{\Phi}_2$, $\mathbf{\Phi}_3$, and $\mathbf{\Phi}_4$ are block matrices; their detailed expressions are as follows:

$$\mathbf{\Phi}_1 = \begin{pmatrix} \mathbf{A}_0 & & \mathbf{0} \\ & \mathbf{A} & \\ \mathbf{0} & & \mathbf{A}_J \end{pmatrix}, \tag{3.11}$$

$$\mathbf{\Phi}_2 = \begin{pmatrix} \mathbf{B}_0 & & \mathbf{0} \\ & \mathbf{B} & \\ \mathbf{0} & & \mathbf{B}_K \end{pmatrix}, \tag{3.12}$$

$$\mathbf{\Phi}_3 = \begin{pmatrix} \mathbf{C}_0 & & \mathbf{0} \\ & \mathbf{C} & \\ \mathbf{0} & & \mathbf{C}_K \end{pmatrix}, \tag{3.13}$$

$$\mathbf{\Phi}_4 = \begin{pmatrix} \mathbf{D}_0 & & \mathbf{0} \\ & \mathbf{D} & \\ \mathbf{0} & & \mathbf{D}_J \end{pmatrix}, \tag{3.14}$$

The iterative algorithm of the IADI solution is as follows:

Algorithm: IADI scheme with unconditional stability

Output: Predicted variables at different space and time domains (x_j, z_k, t_n): $(u^n_{1jk}, u^n_{2jk}, ..., u^n_{mjk})$.

Input: Create time and space nodes J, K, N, time and space steps τ, h_x, h_z, mesh ratios h_x, h_z, and the parameters of the model $a_{12}, a_{23}, ..., a_{(m-1)m}$, $b_{11}, b_{22}, ..., b_{mm}$, $c_{11}, c_{22}, ..., c_{mm}$.

1. Set the initial condition at time $t = 0$ according to Eq. (2.9).
2. Establish the matrices of the boundary conditions $\mathbf{A}_0, \mathbf{A}_J, ..., \mathbf{D}_0, \mathbf{D}_J$.
3. According to Eq. (3.3) and Eq. (3.6), install the matrices of model equations **A**, **B**, **C**, **D**.
4. Assemble the matrices $\mathbf{\Phi}_1$, $\mathbf{\Phi}_2$, $\mathbf{\Phi}_3$, and $\mathbf{\Phi}_4$.
5. **for** n from 1 to N do
   - (I) Set the column vector of external load $\boldsymbol{Q}$
   - (II) Introduce an L-U decomposition method (Chu & Ju, 2013)
   - (III) $\mathbf{\Phi}_1\mathbf{U} = \mathbf{\Phi}_2\mathbf{V} + \mathbf{Q}$
   - (IV) Reconstruct the **U** matrix
   - (V) $\mathbf{\Phi}_3\mathbf{V} = \mathbf{\Phi}_4\mathbf{U} + \mathbf{Q}$
   - (VI) Reconstruct the **V** matrix

   Return III
6. **end**

4. Algorithm application

4.1. Single-phase problem

In this section, the consolidation equation for saturated soil is employed to facilitate comparative verification and to investigate the influence of boundary conditions on the model. This equation was originally established by Terzaghi and has since been extensively studied and applied by researchers and engineers. The consolidation equation for saturated soil is presented as follows (Terzaghi, 1943):

$$\frac{\partial u_1}{\partial t} = b_{11}\frac{\partial^2 u_1}{\partial x^2} + c_{11}\frac{\partial^2 u_1}{\partial z^2} + f_1\frac{\partial f(x,z,t)}{\partial t}. \tag{4.1}$$

Consider a single-layer soil of thickness H and length L subjected to a uniformly distributed loading. These parameters are as follows: $c_{11} = 5 \times 10^{-8}\,\mathrm{m/s^2}$, $k_{xz} = b_{mm}/c_{mm}$, $f_1 = 1$, $f(x,z,t) = 100\,\mathrm{kPa}$, $u_1^0 = 100\,\mathrm{kPa}$, $L = 2\,\mathrm{m}$, $H = 5\,\mathrm{m}$. The bottom boundary of the model is impermeable (NB), while the lateral and upper boundaries are permeable (DB). Before the iteration process, it is advisable to choose as large a grid as possible to minimize the computation time. In addition, the IADI algorithms are developed using MATLAB 2020a[1], and the computer has 16 GB of RAM.

Figure 4 illustrates the time evolution of u_1 and its distribution in the x-z plane under different k_{xz}. For comparison and validation, the computational results from Huang *et al.* (2023) are also included in this figure. As can be observed, the IADI solution proposed in this study agrees well with the analytical solution, demonstrating that the developed solution can effectively capture the characteristics of u_1 (which include pressure distribution and evolution behavior). In Fig. 4a, a large k_{xz} leads to an increased dissipation rate of u_1, causing u_1 to decay more rapidly from its initial value to zero. In Fig. 4b, k_{xz} not only influences the dissipation rate of u_1 but also affects its spatial distribution in the x-z plane. When the coefficient in the x-direction is smaller than that in the z-direction ($b_{11} < c_{11}$), the pressure is primarily released along the z-direction, with only a minor portion released along the x-direction. Furthermore, the release path also exerts a certain influence on pressure dissipation (e.g., $k_{xz} = 1$). Figure 5 demonstrates the effect of different boundary types on the x-z plane distribution of u_1 (u_1 for time $t = 10^6\,\mathrm{s}$). The DB boundary imposes no hindrance on pressure release; the NB boundary completely impedes pressure release; and the RB boundary, which lies between the DB and NB boundaries, partially obstructs the pressure release. The boundary type significantly affects the distribution of u_1.

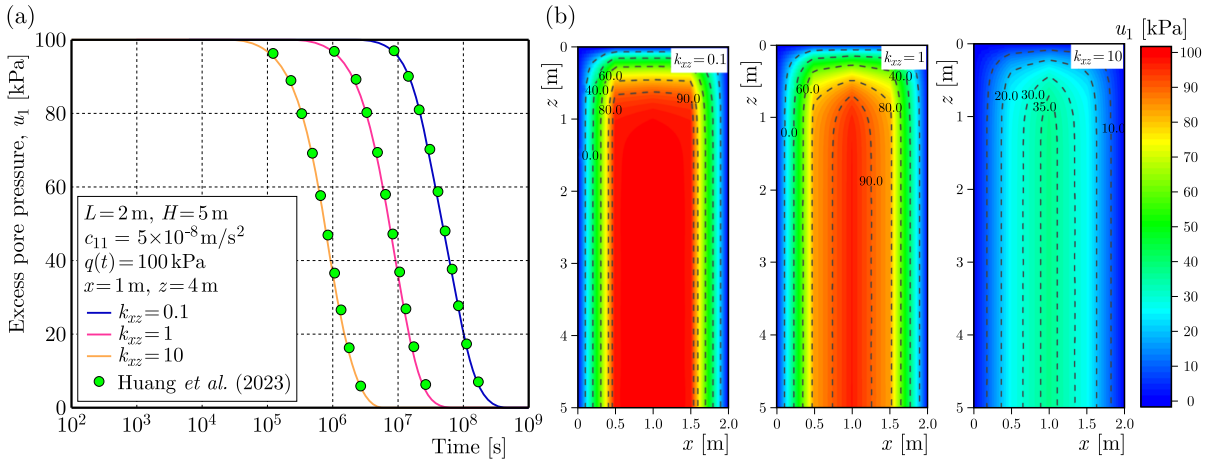


Fig. 4. (a) variation of u_1 under different values of k_{xz}; (b) distribution of u_1 at time $t = 10^6\,\mathrm{s}$.

[1]MATLAB R2020a was developed and released in 2020.

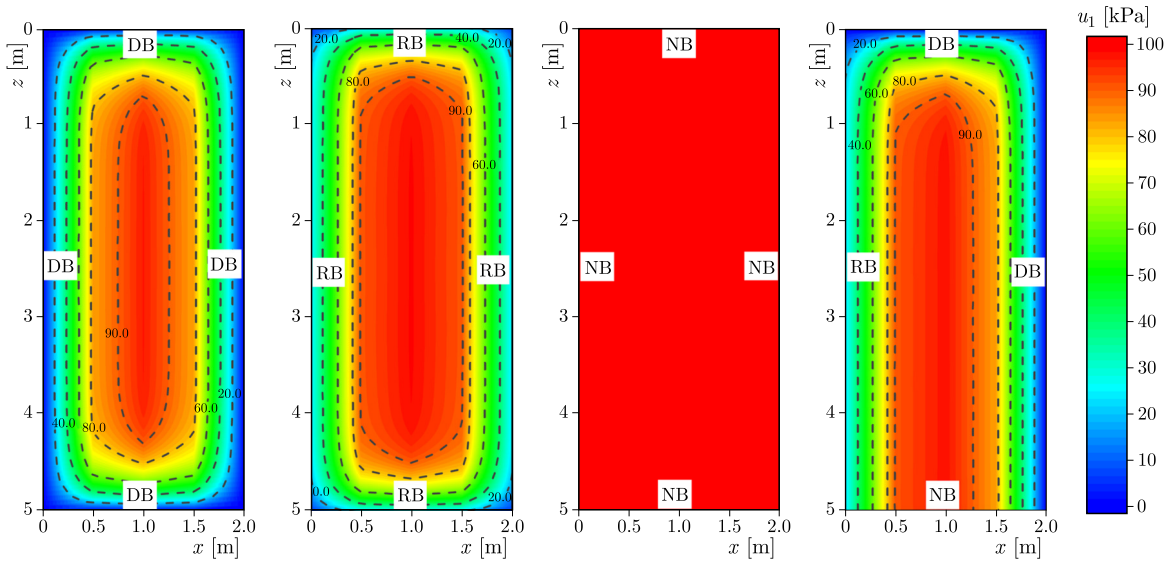


Fig. 5. 2D plot of u_1 under different boundary conditions.

4.2. Two-phase problem

In the context of two-phase coupling problems, the developed IADI algorithm is employed to solve the consolidation equation for unsaturated soil established by Fredlund and Hasan (1979). This equation describes the coupling between air pressure and water pressure, as well as the transient flow of the air and water phases. The consolidation equation for unsaturated soil is presented as follows:

$$\mathbf{E}\frac{\partial \mathbf{u}}{\partial t} = \mathbf{X}\frac{\partial^2 \mathbf{u}}{\partial x^2} + \mathbf{Z}\frac{\partial^2 \mathbf{u}}{\partial z^2} + \frac{\partial \mathbf{f}}{\partial t}, \tag{4.2}$$

where

$$\mathbf{u} = \begin{bmatrix} u_1(x,z,t) \\ u_2(x,z,t) \end{bmatrix}, \qquad \mathbf{E} = \begin{pmatrix} 1 & a_{12} \\ a_{21} & 1 \end{pmatrix}, \qquad \mathbf{X} = \begin{pmatrix} b_{11} & 0 \\ 0 & b_{22} \end{pmatrix},$$

$$\mathbf{Z} = \begin{pmatrix} c_{11} & 0 \\ 0 & c_{22} \end{pmatrix}, \qquad \mathbf{f} = \begin{bmatrix} f_1 \\ f_2 \end{bmatrix} f(x,z,t).$$

The consolidation parameters are as follows: $a_{12} = -0.07538$, $a_{21} = 0.5$, $k_{xz} = b_{mm}/c_{mm}$, $c_{11} = 5.3476 \times 10^{-6}\,\mathrm{m/s^2}$, $c_{22} = 5.102 \times 10^{-8}\,\mathrm{m/s^2}$, $k_{xz} = 1$, $f_1 = 0.1508$, $f_2 = 0.25$, $f(x,z,t) = 100\,\mathrm{kPa}$, $u_1^0 = 20\,\mathrm{kPa}$, $u_2^0 = 40\,\mathrm{kPa}$, $L = 2\,\mathrm{m}$, $H = 4\,\mathrm{m}$. Figure 6 shows the variation and distribution of u_1 under different k_{xz}. The predicted results of the analytical solution from Shen *et al.* (2021) were also plotted in the graph to verify the accuracy of IADI. As observed, the dissipation characteristics of pore pressure in Subsection 4.2 follow the same trend as those in Subsection 4.1. Figure 6a shows the variations of u_1 and u_2 under different values of k_{xz}. With the increase in k_{xz}, the dissipation rate of pore pressure accelerates. The difference lies in the dissipation mode of excess pore pressures associated with u_2, which exhibits distinct behavior due to the coupling between u_1 and u_2 in Eq. (4.2). A comparison of the dissipation curves of u_1 and u_2 reveals that when u_1 begins to decrease, u_2 also decreases. Only after u_1 has completely dissipated does u_2 enter a plateau stage (He *et al.*, 2026b), following which u_2 dissipates independently and slowly to zero. In other words, in a two-phase coupled problem, the release of pore pressure occurs in stages, owing to the difference in the dissipation coefficients, b_{11}, b_{22}, c_{11} and c_{22} (Phase I: u_1 and u_2 dissipation; Phase II: only u_2 dissipation, Shan *et al.*, 2012). Figure 6b demonstrates the 2D plots of u_1 and u_2 in the x-z plane (u_1 for time $t = 10^5\,\mathrm{s}$; u_2

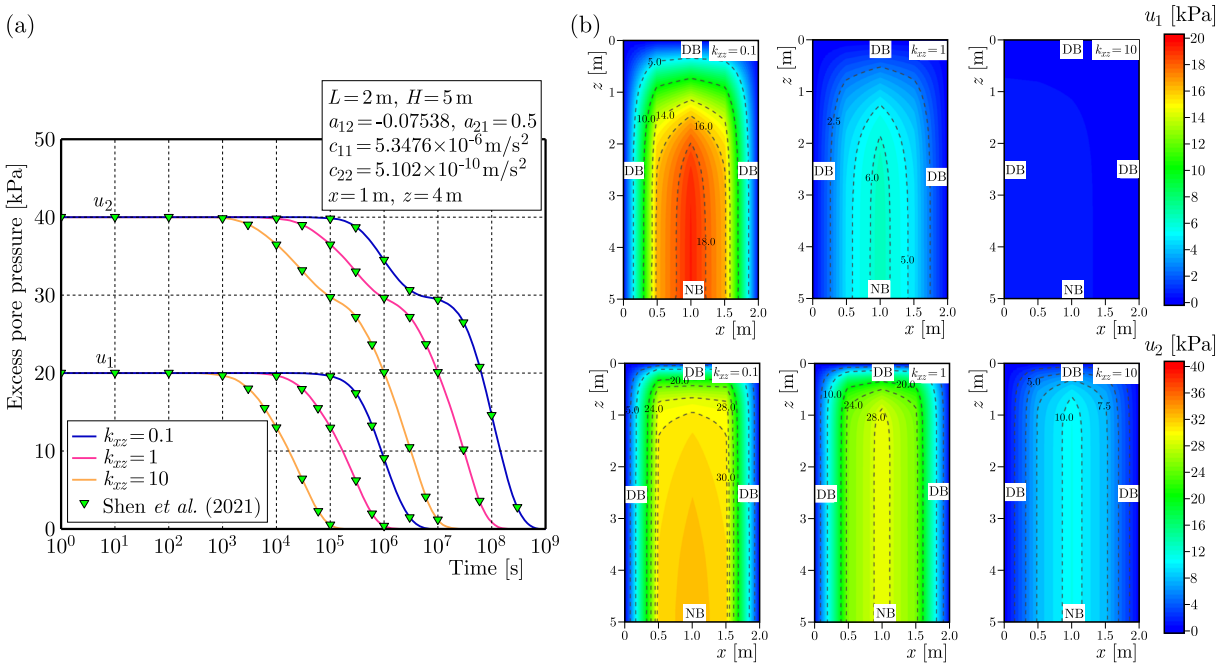


Fig. 6. (a) variations of u_1 and u_2 under different values of k_{xz}; (b) distributions of u_1 and u_2 in the x-z plane.

for time $t = 5 \times 10^6\,\mathrm{s}$). The distributions of u_1 and u_2 are similar, with a significant influence from boundary conditions. The distribution patterns of u_1 and u_2 also demonstrate that the developed IADI algorithm is accurate.

4.3. Three-phase problem

A three-phase coupling problem is considered, and the system of partial differential equations is given as follows:

$$\mathbf{E}\frac{\partial \mathbf{u}}{\partial t} = \mathbf{X}\frac{\partial^2 \mathbf{u}}{\partial x^2} + \mathbf{Z}\frac{\partial^2 \mathbf{u}}{\partial z^2} + \frac{\partial \mathbf{f}}{\partial t}, \tag{4.3}$$

where

$$\mathbf{u} = \begin{bmatrix} u_1(x,z,t) \\ u_2(x,z,t) \\ u_3(x,z,t) \end{bmatrix}, \quad \mathbf{E} = \begin{pmatrix} 1 & a_{12} & a_{13} \\ a_{21} & 1 & a_{23} \\ a_{31} & a_{32} & 1 \end{pmatrix}, \quad \mathbf{X} = \begin{pmatrix} b_{11} & 0 & 0 \\ 0 & b_{22} & 0 \\ 0 & 0 & b_{33} \end{pmatrix},$$

$$\mathbf{Z} = \begin{pmatrix} c_{11} & 0 & 0 \\ 0 & c_{22} & 0 \\ 0 & 0 & c_{33} \end{pmatrix}, \quad \mathbf{f} = \begin{bmatrix} f_1 \\ f_2 \\ f_3 \end{bmatrix} f(x,z,t).$$

These parameters are as follows: $a_{12} = a_{23} = 0.5$, $a_{31} = -0.5$, $a_{13} = a_{21} = a_{32} = 0$, $b_{11} = k_{xz}c_{11} = 5.0\times10^{-6}$, $b_{22} = k_{xz}c_{22} = 5.0\times10^{-7}$, $b_{33} = k_{xz}c_{33} = 5.0\times10^{-8}$, $c_{11} = 5.0\times10^{-6}$, $c_{22} = 5.0\times10^{-7}$, $c_{33} = 5.0\times10^{-8}$, $k_{xz} = 1$, $f_1 = f_2 = f_3 = 0$, $f(x,z,t) = 100\,\mathrm{kPa}$, $u_1^0 = 10\,\mathrm{kPa}$, $u_2^0 = 20\,\mathrm{kPa}$, $u_3^0 = 40\,\mathrm{kPa}$, $L = 2\,\mathrm{m}$, $H = 4\,\mathrm{m}$. The boundary conditions of the model are considered as Dirichlet boundaries. In three-phase coupling problems, the pressure dissipation patterns exhibit multi-stage characteristics due to variations in parameters. In this section, to validate the stability of the proposed IADI algorithm, the three-phase coupling problem is solved using the IADI scheme with different mesh ratios. Table 1 presents the computational results and the corresponding CPU time obtained with various mesh ratios. It is observed that as the time step size increases, the IADI algorithm maintains excellent stability in its computed

Table 1. Calculation time and results under different time steps.

Time step [s]	Calculation time [s]	$z = 1\,\mathrm{m}$			$z = 2\,\mathrm{m}$			$z = 3\,\mathrm{m}$		
		u_1 [kPa]	u_2 [kPa]	u_3 [kPa]	u_1 [kPa]	u_2 [kPa]	u_3 [kPa]	u_1 [kPa]	u_2 [kPa]	u_3 [kPa]
1	345.45	0.30	7.17	33.46	0.39	8.89	34.03	0.30	7.17	33.46
10	38.36	0.30	7.17	33.46	0.39	8.89	34.03	0.30	7.17	33.46
100	4.47	0.30	7.17	33.46	0.39	8.89	34.03	0.30	7.17	33.46
1000	0.58	0.30	7.16	33.45	0.39	8.89	34.03	0.30	7.16	33.45

Note: $t_N = 10^8\,\mathrm{s}$; $h_x = 0.125$, $h_z = 0.25\,\mathrm{m}$, $x = 1\,\mathrm{m}$.

results. Furthermore, a larger mesh ratio leads to higher computational efficiency. These findings demonstrate that the IADI algorithm developed in this study possesses high computational efficiency and accuracy, rendering it well-suited for solving multidimensional coupled problems.

5. Conclusion

On the basis of the heat conduction equation, the consolidation equation for saturated soils, and the consolidation equation for unsaturated soils, this paper proposes a system of multiphase-coupled parabolic PDEs. Then, an IADI solution is presented to solve this system of PDEs with multiple physical quantities. The reliability and accuracy of the proposed numerical method are also verified by comparing the results of the numerical and existing analytical solutions. The results show that the developed numerical solution has higher computational efficiency and more convenient programs. Therefore, it is relatively easier to execute a preliminary assessment for the multiphase coupling problem.

Acknowledgments

This study was funded by the National Natural Science Foundation of China (Grant No. 42277149), Natural Science Foundation of Sichuan (Grant No. 2022NSFSC0443), and Research Project of Sichuan Provincial Department of Education (Grant No. 15ZA0138).

References

1. Chu, B.Z., & Ju, C.H. (2013). Forward elimination and backward substitution algorithm for solving block pentadiagonal linear equations (in Chinese). *Pure Mathematics*, *3*, 139–143. http://doi.org/10.12677/pm.2013.32022
2. Dakshanamurthy, V., & Fredlund, D.G. (1980). Moisture and air flow in an unsaturated soil. In D. Snethen (Ed.), *Proceedings of the Fourth International Conference on Expansive Soils* (pp. 514–532). ASCE.
3. Feng, J.X., Ni, P.P., & Mei, G.X. (2019). One-dimensional self-weight consolidation with continuous drainage boundary conditions: Solution and application to clay-drain reclamation. *International Journal for Numerical and Analytical Methods in Geomechanics*, *43*(8), 1634–1652. https://doi.org/10.1002/nag.2928
4. Fredlund, D.G., & Hasan, J.U. (1979). One-dimensional consolidation theory: unsaturated soils. *Canadian Geotechnical Journal*, *16*(3), 521–531. https://doi.org/10.1139/t79-058
5. He, Q., Li, L.Q., Dong, C.H., & Li, T. (2026a). Three-dimensional consolidation of unsaturated soil with anisotropic permeability considering mixed drainage boundary condition. *Mechanics of Solids*, *61*, Article 78. https://doi.org/10.1134/S0025654425607190

6. He, Q., Li, L.Q., Yuan, Q., & Yang, Y.H. (2026b). Implicit difference solution for position optimization of a sand cushion in the double-layered unsaturated soil ground. *International Journal of Geomechanics*, *26*(9), Article 04026172. http://doi.org/10.1061/IJGNAI.GMENG-13347
7. He, Q., Yuan, Q., & Lang, L. (2025a). A fast and robust numerical solution for the position design of horizontal drains in a saturated-unsaturated soil ground system. *Journal of Theoretical and Applied Mechanics*, *63*(4), 839–853. https://doi.org/10.15632/jtam-pl/203694
8. He, Q., Yuan, Q., Lang, L., & Cao, J.X. (2025b). Implicit difference solution for one-dimensional consolidation of unsaturated soil: Numerical verification and application to soil-cushion system. *Mathematical Geosciences*, *57*(5), 951–976. https://doi.org/10.1007/s11004-025-10177-6
9. Huang, R., Ni, P.P., Yang, W.T., Chen, Z., Dong, Q.X., & Mei, G.X. (2023). Semianalytical solution for consolidation of reclaimed land with horizontal drains. *International Journal of Geomechanics*, *23*(4), Article 04023010. https://doi.org/10.1061/IJGNAI.GMENG-7921
10. Kou, H., Shi, Z., Zhao, Y.Z., Li, J., & Wang, Q. (2026). A two-dimensional transformed differential quadrature solution for air-hydro-mechanical coupling in layered unsaturated soils. *International Journal for Numerical and Analytical Methods in Geomechanics*, *50*(5), 2189–2205. https://doi.org/10.1002/nag.70202
11. Morton, K.W., & Mayers, D.F. (2005). *Numerical solution of partial differential equations*. Cambridge University Press. https://doi.org/10.1017/CBO9780511812248
12. Myers, T.G., Hennessy, M.G., & Calvo-Schwarzwälder, M. (2020). The Stefan problem with variable thermophysical properties and phase change temperature. *International Journal of Heat and Mass Transfer*, *149*, Article 118975. https://doi.org/10.1016/j.ijheatmasstransfer.2019.118975
13. Perthame, B. (2015). *Parabolic equations in biology: Growth, reaction, movement and diffusion*. Springer. https://doi.org/10.1007/978-3-319-19500-1
14. Shan, Z.D., Ling, D.S., & Ding, L.H. (2012). Exact solutions for one-dimensional consolidation of single layer unsaturated soil. *International Journal for Numerical and Analytical Methods in Geomechanics*, *36*(6), 708–722. https://doi.org/10.1002/nag.1026
15. Sharifi, S., & Rashidinia, J. (2016). Numerical solution of hyperbolic telegraph equation by cubic B-spline collocation method. *Applied Mathematics and Computation*, *281*, 28–38. https://doi.org/10.1016/j.amc.2016.01.049
16. Shen, S.D., Wang, L., Zhou, A.N., Xu, Y.F., & Xia, X.H. (2021). Two-dimensional plane strain consolidation for unsaturated soils with a strip-shaped distributed permeable boundary. *Computers and Geotechnics*, *137*, Article 104273. https://doi.org/10.1016/j.compgeo.2021.104273
17. Singh, A., & Chakraborty, M. (2024). Combined effect of non-Darcian flow and semipermeable drainage boundaries on one-dimensional consolidation of unsaturated soil. *International Journal of Geomechanics*, *24*(8), Article 04024157. https://doi.org/10.1061/IJGNAI.GMENG-9659
18. Terzaghi, K. (1943). *Theoretical soil mechanics*. John Wiley and Sons, Inc. https://doi.org/10.1002/9780470172766
19. Thomas, J.W. (1995). *Numerical partial differential equations: Finite difference methods*. Springer. https://doi.org/10.1007/978-1-4899-7278-1
20. Wang, L., Xu, Y.F., Xia, X.H., He, Y.L., & Li, T.Y. (2019). Semi-analytical solutions to two-dimensional plane strain consolidation for unsaturated soils under time-dependent loading. *Computers and Geotechnics*, *109*, 144–165. https://doi.org/10.1016/j.compgeo.2019.01.002
21. Yuan, Q., He, Q., Lang, L., & Yang, X.B. (2023). Analytical solution for Fredlund–Hasan unsaturated consolidation using mode superposition method. *International Journal for Numerical and Analytical Methods in Geomechanics*, *47*(17), 3234–3247. https://doi.org/10.1002/nag.3618
22. Zhou, W.H., & Zhao, L.S. (2014). One-dimensional consolidation of unsaturated soil subjected to time-dependent loading with various initial and boundary conditions. *International Journal of Geomechanics*, *14*(2), 291–301. https://doi.org/10.1061/(ASCE)GM.1943-5622.0000314

Manuscript received June 2, 2026; accepted for publication September 22, 2026; published online November 6, 2026.